International journal of COMADEM
Vol # No # (January 2022) p.##-##

COMADEM

International Journal of Condition Monitoring and Diagnostic Engineering Management

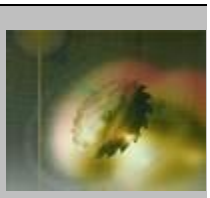

Aerodynamic analysis of a car-trailer combination using CFD based numerical techniques: A shape optimisation and drag reduction study

Muhammad Atif [a]*, Aliyu M Aliyu [b], Rakesh Mishra [a]

[a] *University of Huddersfield, HD1 3DH, United Kingdom*
[b] *University of Lincoln, LN6 7TS , United Kingdom*
∗ *Muhammad Atif, Tel.: +447565935968; email: Muhammad.atif@hud.ac.uk*

ABSTRACT

The concept of towable horse trailers and caravans has become increasingly common for transporting horses around the country as well as for providing a comfortable and mobile living space during vacations. It is very common for the towing vehicle to double its fuel usage by towing a horse trailer or a caravan. The massive increase in fuel consumption is mainly due to the changed aerodynamics. To optimise the design of the trailer and reduce fuel consumption, it is essential to know the high drag contribution surfaces and appropriately modifying them. In the present study, two different industrial models of the horse-trailer have been evaluated and optimised for their aerodynamic drag. Both trailers have a different front design which can represent almost all-important feature changes to estimate the drag contribution and prediction of the best-optimised shape. The challenge is to reduce the drag force without reducing the internal accommodation space and meeting the legal specifications. The front shape of the trailer, roof and different add-on devices has been tested and drag performance has been evaluated. The length of the wake region has been improved by providing a roof curvature and diffuser at the top and bottom rear side of the trailer. Providing a roof curvature on the trailer roof has delayed the flow separation at the rear end of the roof by reducing the adverse pressure gradients. The wake behind the car is found sensitive to the gap between the car and trailer. Adverse pressure gradient has been recovered in the wake region by using add-on devices. This resulted in the conclusion that fuel consumption has been reduced to a significant percentage.

Keywords: *Horse Trailer; Drag Force; Computational Fluid Dynamics CFD.*
Article history: *Received ; Published .*

1. Introduction

A livestock trailer is an unpowered vehicle used to transport live animals such as cattle and horses. Horse trailers were initially used solely to transport horses around cities but were later developed to accommodate up to two adults in the living area at the front of the trailer and two horses in the horse area of the trailer. The addition of human accommodation has constrained the front shape of the trailer. A compromise between the living space and aerodynamics is essential, hence it is important to design more aerodynamic and fuel-efficient trailers. Moreover, the addition of an accommodation facility has increased the length of the trailer which in turn increases the drag force on the trailer. It is very common to double the fuel consumption of the vehicle by towing a trailer or caravan [1]. In the early years, when the fuel prices were low and supply was sufficient, vehicles were designed with an aesthetic appearance and more space. Rising fuel prices and global warming effects have encouraged research into investigating different aerodynamic shape adaptations in order to reduce both drag force and fuel consumption. The power required to overcome drag is proportional to the cube of the free stream velocity of the vehicle, which means a significant amount of fuel is used to overcome drag on the highways [2].

To enhance the fuel efficiency of the vehicle-trailer assembly, it is necessary to redesign the important aerodynamic design features of the horse trailer which can improve streamlined flow. Comprehensive studies were carried out on the ventilation of caravans, horse trailers and livestock trailers. Few studies however have been published in the field of design optimisation of towing trailers [1]. A car-trailer assembly consists of two bluff bodies which complicate the flow phenomenon. Boxed shaped design and the sharp frontal edges generate uneven pressure distribution on the body of the trailer. This uneven pressure drop causes the early flow separation [3, 4]. The effect of rounding and trimming the frontal edge and providing a slant on the frontal face has a similar influence on the drag force [5]. However, the latter approach reduces the internal space in the living area inside the trailer. The airflow over the car-trailer assembly can also be improved by modifying the shape of the towing vehicle. A significant drag reduction is observed by placing a deflector plate on the car at a specific distance and angle. The gap region between the car and trailer also contributes significant drag and requires devices that can direct the flow efficiently on the roof of the trailer without causing high flow recirculation in the gap region [6].

The aerodynamic efficiency of add-on devices and design improvements are some of the opportunities in this field. In view of this opportunity, this study seeks to explore two different commercial horse trailer models with inside accommodation . In the first phase of the analysis, the drag force and drag coefficient have been examined and compared numerically using CFD software and design optimisation has been carried in the

second phase of the analysis. A four-by-four towing vehicle model has been used for the analysis and the design of this towing vehicle is kept constant throughout the analysis. The front and rear faces of both trailers are found to be the major contributors to the drag. Different front face fillets are simulated to investigate the effect of the drag force. Three front face heights where the leading-edge curvature starts, are simulated to find the optimum depth of the fillet curve on the frontal edge. The roof camber effect is tested on one of the models by changing a control parameter h/l (here h=maximum height of the curve from a horizontal line passing through the endpoints of the curve, l=length of the curve). Length of the wake region is another important parameter that is optimised in this study. Add-on devices like diffusers are tested at different angles to reduce the wake region length. A significant reduction in drag force and fuel consumption has been achieved due to the novel modifications proposed in this study.

1. Theoretical Background

A vehicle on-road may encounter three forms of fluid forces: drag, lift and side force. Depending on the yaw angle of the resultant velocity of the vehicle and wind, the flow encounter can be either headwind or crosswind. In a headwind flow, both, the vehicle and the wind move along the same axis and have a zero-yaw angle. In this case, the side force for asymmetric shape is almost zero. The drag force experienced by a vehicle is a blend of frictional, interference, and pressure drag as it travels through a fluid. Pressure drag is, however, the most significant drag force experienced by the vehicle, accounting for more than 90% of the total drag force [7]. Drag force can be measured by performing either full-scale or small-scale experiments in the wind tunnel or by using the CFD analysis tools. A non-dimensional number known as drag coefficient is computed using the drag force, velocity, density and frontal area information of the vehicle and it is used to compare the performance of similar geometries but having different features. It depends on the amount of turbulence in the flow and the projected area of the vehicle [8].

$$\text{Drag coefficient} = C_d = \frac{F_d}{\frac{1}{2} \times \rho {v_\infty}^2 A} \quad (1)$$

Here, C_d, F_d, ρ,v and A are the drag coefficient, drag force, the density of the air, the free stream velocity and the frontal/projected area of the object respectively. Vehicles can also encounter lift force (FL) and side force (Fs) which are compared for different geometries by dimensionless numbers known as lift coefficient C_L and side coefficient C_s.

$$\text{Lift force coefficient} = C_L = \frac{F_L}{\frac{1}{2} \times \rho {v_\infty}^2 A} \quad (2)$$

$$\text{Side force coefficient} = C_s = \frac{F_s}{\frac{1}{2} \times \rho {v_\infty}^2 A} \quad (3)$$

Vehicles rarely move alone on the road and they either follow another vehicle or they cross each other on the highways or country roads[9]. The flow field of every vehicle is influenced by the other vehicles and the interference of the flow fields take place. In the tractor-trailers, caravans and horse trailers the two bodies are very close to each other. The sum of the individual drag of a car and a trailer is not necessarily equal to the combined drag of the configuration. The difference in the drag of the two interactive bodies is called interference of drag [9, 10]. However, the mutual effects of the interference are multifaceted and the flow over a bluff body can benefit from the lee-side effect. Due to the wake flow produced by the leading body, the pressure rise is moderate in front of the following body, which helps in the reattachment of the flow. As a result of this, the drag on the second body is reduced. This effect is known as the lee-side effect[9].

$$\Delta D = D_{car+trailer} - (D_{car} + D_{trailer}) \quad (4)$$

Developing an experimental wind tunnel setup takes longer and costs lots of money to determine all these forces. Numerical techniques such as CFD are effectively employed in predicting the solid-liquid interaction and determining the forces very close to the experimental data. The CFD has become an integrated part of Research and Development by saving time and money on various industrial problems. The CFD can produce a visual representation of a wide range of local flow field variables such as velocity, pressure, turbulence and vorticity. Using CFD codes, on the other hand, isn't necessarily the cheapest or fastest solution. It requires a certain level of competency to trust confidently the data projected by the CFD codes. The most time-consuming phase in CFD analysis is creating a decent mesh and setting boundary conditions that are a true representation of the physical phenomenon [11].

1.1. Reynolds-Averaged Navier Stokes (RANS) Model

A variety of modelling techniques have been developed over time for computational fluid dynamics. Unsteady Reynolds-Averaged Navier Stokes equation (URANS), large eddy simulation (LES), detached large eddy simulation (DES), hybrid LES/RANS model, and Direct Numerical Simulation (DNS) are some of these models [12]. The RANS model is based on the Reynolds decomposition of the Navier-Stokes equation. In incompressible flow, the Navier–Stokes and continuity equations for three-dimensional motion is described by a set of partial differential equations which are mathematical representations of the conservation of mass and momentum. Equations 5 – 7 [10] show the inter-relation between pressure and velocity in x, y and z-direction respectively.

$$\rho\left[\frac{\partial u}{\partial t} + \frac{\partial (u^2)}{\partial x} + \frac{\partial (uv)}{\partial y} + \frac{\partial (uw)}{\partial z}\right] = -\frac{\partial p}{\partial x} + \mu\left[\frac{\partial^2 u}{\partial x^2} + \frac{\partial^2 u}{\partial y^2} + \frac{\partial^2 u}{\partial z^2}\right] + S_u \quad (5)$$

$$\rho\left[\frac{\partial v}{\partial t} + \frac{\partial (uv)}{\partial x} + \frac{\partial (v^2)}{\partial y} + \frac{\partial (vw)}{\partial z}\right] = -\frac{\partial p}{\partial y} + \mu\left[\frac{\partial^2 v}{\partial x^2} + \frac{\partial^2 v}{\partial y^2} + \frac{\partial^2 v}{\partial z^2}\right] + S_v \quad (6)$$

$$\rho\left[\frac{\partial w}{\partial t} + \frac{\partial (wu)}{\partial x} + \frac{\partial (wv)}{\partial y} + \frac{\partial (w^2)}{\partial z}\right] = -\frac{\partial p}{\partial z} + \mu\left[\frac{\partial^2 w}{\partial x^2} + \frac{\partial^2 w}{\partial y^2} + \frac{\partial^2 w}{\partial z^2}\right] + S_w \quad (7)$$

Here, ρ is the density of the fluid, t is the time, p is pressure and μ is the dynamic viscosity. RANS model is based on the NS equations but the solution includes mean and fluctuation parts. The mean of the NS equation forms Reynolds stress tensor which rises the closure problem and this requires a modelling approach to estimate the solution of the equation [13]. The dependent variable in the NS equation is replaced by mean ($\bar{u}$ $\bar{v}$ $\bar{w}$ and $\bar{p}$) and fluctuating parts ($u'v'$ w' and p'). In the RANS model, average motion is computed and fluctuations are modelled. After replacing the dependent variable with mean and fluctuating parts, the NS equations transform into RANS equations as given below: [13]

$$u=\bar{u}+u' \quad (8)$$

$$u=\bar{u}+u' \quad (9)$$

$$w=\bar{w}+w' \quad (10)$$

$$p=\bar{p}+p' \tag{11}$$

$$\bar{u}\frac{\partial \bar{u}}{\partial x}+\bar{v}\frac{\partial \bar{u}}{\partial y}+\bar{w}\frac{\partial \bar{u}}{\partial z}=-\frac{1}{\rho}\frac{\partial \bar{p}}{\partial x}+\frac{\mu}{\rho}\left[\frac{\partial^2 \bar{u}}{\partial x^2}+\frac{\partial^2 \bar{u}}{\partial y^2}+\frac{\partial^2 \bar{u}}{\partial z^2}\right]+\left[\frac{\partial \overline{u'u'}}{\partial x}+\frac{\partial \overline{u'v'}}{\partial y}+\frac{\partial \overline{u'w'}}{\partial z}\right] \tag{12}$$

$$\bar{u}\frac{\partial \bar{v}}{\partial x}+\bar{v}\frac{\partial \bar{v}}{\partial y}+\bar{w}\frac{\partial \bar{v}}{\partial z}=-\frac{1}{\rho}\frac{\partial \bar{p}}{\partial y}+\frac{\mu}{\rho}\left[\frac{\partial^2 \bar{v}}{\partial x^2}+\frac{\partial^2 \bar{v}}{\partial y^2}+\frac{\partial^2 \bar{v}}{\partial z^2}\right]+\left[\frac{\partial \overline{u'v'}}{\partial x}+\frac{\partial \overline{v'v'}}{\partial y}+\frac{\partial \overline{v'w'}}{\partial z}\right] \tag{13}$$

$$\bar{u}\frac{\partial \bar{w}}{\partial x}+\bar{v}\frac{\partial \bar{w}}{\partial y}+\bar{w}\frac{\partial \bar{w}}{\partial z}=-\frac{1}{\rho}\frac{\partial \bar{p}}{\partial z}+\frac{\mu}{\rho}\left[\frac{\partial^2 \bar{w}}{\partial x^2}+\frac{\partial^2 \bar{w}}{\partial y^2}+\frac{\partial^2 \bar{w}}{\partial z^2}\right]+\left[\frac{\partial \overline{u'w'}}{\partial x}+\frac{\partial \overline{v'w'}}{\partial y}+\frac{\partial \overline{w'w'}}{\partial z}\right]-g \tag{14}$$

1.2. Turbulence Modelling

Most real-life flows are turbulent and it is impossible to resolve the fluctuation of physical phenomena to their smallest units in time and space using analytical methods [14]. As a result, time averaged quantities are used in combination with their fluctuations using the Reynolds decomposition given in Equations (8)–(11). The fluctuating terms after substituting into the Navier – Stokes equations produce the terms on the right hand side of Equations (12)–(14) known as the Reynolds stresses which are computationally expensive to be calculated directly. This gives rise to the concept of turbulence modelling where they are replaced by empirically determined expressions called turbulence models. Turbulence models can be categorised into two groups; one of them is based on the eddy viscosity concept and the other is based on the individual turbulence stresses and fluxes. The eddy viscosity concept treats turbulence as isotropic, however, the non-eddy viscosity concept considers the turbulence as anisotropic [5, 15]. The idea behind the transport equation turbulence model is to describe one or more characteristic turbulence scales i.e. kinetic energy and dissipation, with the aid of partial differential equations. The most commonly used model of this class in vehicle aerodynamics are K-Ɛ, K-τ, K-omega and K-omega SST models.[16]

The SST k-ω turbulence model is a type of transport equation model, which is a hybrid model of the K-Ɛ and K-omega models. In the near-wall layers, the K-Ɛ model predicts false results due to the high value of the production term. However, the K-omega model in the inner boundary layers makes it usable to resolve the flow all the way down to the viscous sub-layer. On the other hand, the K-Ɛ model can solve the flow accurately away from the boundary. The combination of these two models provides a successful hybrid model to solve the adverse pressure gradient and separated flows. The kinematic eddy viscosity can be found using the equation[15]:

$$V_T=\frac{a_1 K}{\max\left(a_1 w, SF_{2)}\right)} \tag{15}$$

The turbulence kinetic energy can be found using the equation [16]

$$\frac{\partial k}{\partial t}+U_j\frac{\partial k}{\partial x_j}=P_k-\beta^* k\omega+\frac{\partial}{\partial x_j}\left[(\nu+\sigma_k\nu_T)\frac{\partial k}{\partial x_j}\right] \tag{16}$$

The specific dissipation rate can find out using the equation [17]:

$$\frac{\partial \omega}{\partial t}+U_j\frac{\partial \omega}{\partial x_j}=\alpha S^2-\beta\omega^2+\frac{\partial}{\partial x_j}\left[(\nu+\sigma_\omega\nu_T)\frac{\partial \omega}{\partial x_j}\right]+2(1-F_1)\sigma_{\omega 2}\frac{1}{\omega}\frac{\partial k}{\partial x_i}\frac{\partial \omega}{\partial x_i} \tag{17}$$

1.3. Drag Reduction Techniques

The process of minimization of the drag force involves the reduction of the frictional drag and pressure drag. The frictional drag can be reduced by producing the vehicle with a highly finished surface and continuous surfaces. This can also be achieved by making smooth contours of the vehicle [3]. The gaps, protuberances, extrusions and discontinuities in the surface produce pressure drag, but they will also boost up the frictional drag by increasing the thickness of the boundary layer [18]. A reasonable difference in frictional drag can be achieved by sustaining the boundary layer as laminar[19].

Maintaining a laminar boundary on the whole body of the vehicle is, however, an almost impossible task in a real case. At 62 mph speed, transition on a smooth flat plate starts after 30cm[3]. A favourable pressure gradient will help to reduce the growth of the boundary layer. The underside of the trailers is generally smooth; hence this area does not need sufficient attention for improvement. However, the diffuser or boat tailing technique can be applied to get the advantage of this methodology. The underbody flow influences the wake region which is the main cause of pressure drag. Similar to the boat tailing technique, the recovery of pressure can also be achieved by tapering the bottom of the vehicle upward [18]. Another technique to delay flow separation is to provide the curvature on the roof, which resultantly reduces the drag. Add-on devices such as diffusers can also help to reduce drag if positioned correctly. The leading edge of the trailer plays an important role in flow attachment to the roof of the trailer. Tapering and rounding the leading edge has proven to be efficient in drag reduction.

2. Methodology

The flow analysis is carried using CFD software, Ansys Fluent 17.0. The 3-D designs of the car and horse trailers have been created using SOLIDWORKS. The performance of commercial CFD software for heavy-duty trailers, vehicles, and vehicle-trailer combinations has been evaluated in prior bluff body studies. If the mesh parameters are generated and properly monitored, the drag force result has shown to be in good agreement with the experimental data [14]. In complicated and near-wake sections, a highly-resolved mesh grid is required to capture the pressure gradient correctly and closer to the experimental data [20, 21]. Figure 1 shows the assembly of the car and two different models of the horse trailers named as model X and model Y. The same car design was used with both horse trailer models to compare the effect of shape modification. A 3-D flow field around the trailer was created in the Ansys design modeller. The length, width and height of the domain was kept as 110m, 40m, and 15m respectively. The domain's upstream and downstream lengths were specified at three and seven times the assembly's lengths, respectively. The distance between the trailer's side face and the domain's side face was kept twice the car-trailer length. The height of the flow domain was kept as six times the height of the assembly as in Figure 2. Because the blockage ratio was less than 1%, no blockage correction was performed. In another investigation on tractor-trailers, similar dimensions were selected. [4, 22].

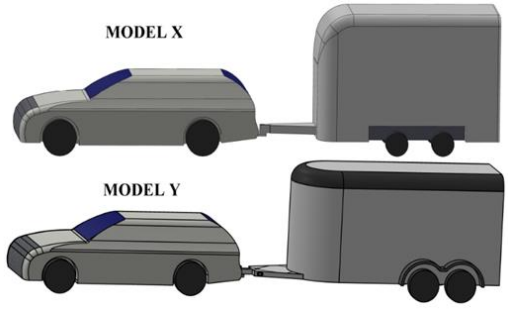

Figure 1 Isometric view of the car-trailer assemblies of model X and Y

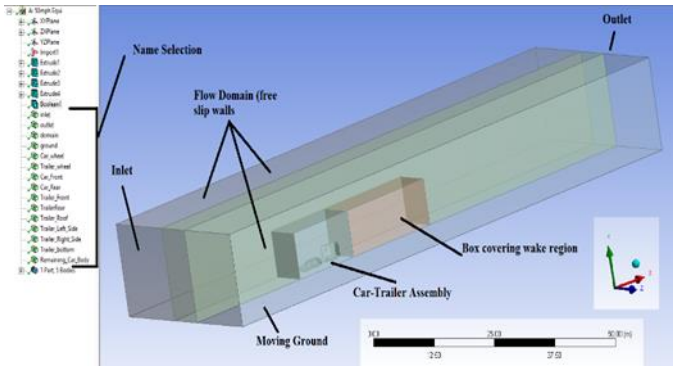

Figure 2 Geometry prepared in ANSYS design modeller

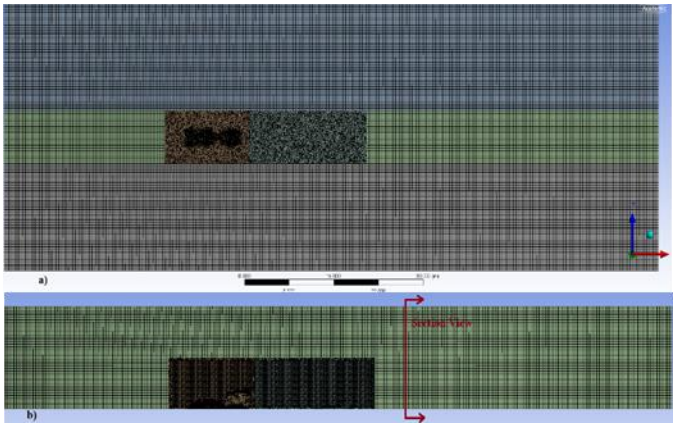

Figure 3 Mesh generated for CFD analysis a) shows the whole domain b) shows section view of the domain

Mesh creation is an important phase in CFD analysis, and the reliability and accuracy of the output is greatly influenced by mesh quality, among other factors. As indicated in Figure 3, the single body domain was further subdivided into five bodies to modify mesh element size individually in each part. One of the bodies was created to cover the car-trailer assembly and another was created to cover the wake region behind the trailer. A highly refined tetrahedron mesh was defined on the two bodies covering the car-trailer assembly and wake region, rest of the domain was discretised using hex elements. This controlled mesh generation technique has reduced the element count as a result, the computational power and time has been reduced without compromising the accuracy of results. Actual vehicle outlines were highly detailed which caused a large number of skewed elements around the car and wheels. To improve the skewness and quality of the mesh, the geometric features of car and trailers causing high skewed cells were refined. A small extrusion was created around the wheels to cover the zero-thickness region created between the wheels and ground interaction. This has improved the skewness and there were no cells with skewness more than 0.9 and 98% of the cells achieved skewness less than 0.7. An inflation layer was created around the car-trailer and ground. However, the layer was not consistent because of complex geometry, curved surfaces and varying feature sizes. A highly refined mesh, however, was created by controlling the element size around the car-trailer assembly to get the Y+ value in the log region at the maximum areas of the car-trailer assembly.

Mesh convergence study has been carried out on both models X and Y to achieve reasonable independence of results from the mesh variation. The number of elements was changed from one million to five million, and the drag results were found to be steady after four million mesh elements, as shown in Figure 4. Moreover, a domain independence study was also carried out using model X to ensure that the drag results are independent of the domain size and there is no reverse flow at the outlet. This will reduce error in the mass conservation equation and help to improve the solution convergence. Table 1 below shows 3 different size combinations of upstream, downstream and bodies covering the wake region. The combinations were simulated using the same mesh control. The first set of parameters was selected for further analysis because the dependency with increasing the size of the domain was less than 1%. However, a larger domain will generate a greater number of elements for the same set of mesh control which will consume more computational power and time without a significant effect on results.

Table 1 Domain independence parameters

Parameter Name	Length	Drag Force	Drag Coefficient
Upstream Length	03 x length	778.95	0.5463
	05 x length	771.95	0.5418
Downstream length	07 x length	778.95	0.5463
	10 x length	785.76	0.5515
	15 x length	787.18	0.5525
Body around the car-trailer assembly	13000mm	778.95	0.5463
	15000mm	772.64	0.5423
Body around the wake region	20000mm	778.95	0.5463
	30000mm	772.41	0.5421

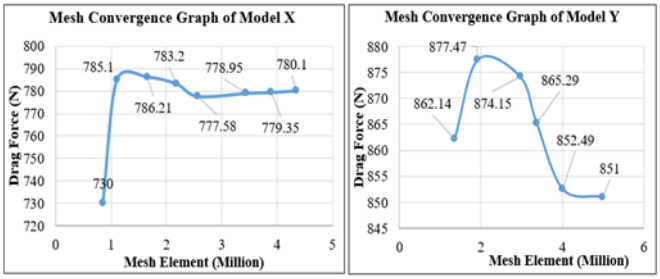

Figure 4 Mesh convergence study of both models

Pressure-based steady flow analysis was used with the settings defined in the table below. The vehicle body was kept stationary and air at 50 mph is set to move from inlet to outlet in +ve x-direction. This was the national speed limit for towing a trailer or caravan on a single carriageway and it was also consistently used in the literature [3]. The ground was set to a moving boundary at the same speed and direction of the flow. The moving ground will prevent the excessive formation of the boundary layer between the lower surface of the car-trailer assembly and the ground. The drag effect of wheels was included by defining the wheel faces as rotating walls. The equivalent rotational speed was calculated using the relationship "v = r x ω" where V= free stream velocity; r = radius of wheels; ω = rotational velocity of wheels. The rest of the domain walls were defined as free slip walls with zero wall shear. The body of the car and trailer was given no-slip conditions, including the viscous effect of flow.

Each face of the car-trailer was defined with a separate name selection which allows calculating drag contribution by each face and to determine critical features for the design optimisation.

Pressure and velocity field in the flow domain and around the car-trailer combination was computed by using Reynolds averaged Navier-Stokes (RANS) equation and continuity equation. The flow is considered as incompressible because at small Mach numbers, the spatial and time rate of change in density can be assumed zero. The RANS equation forms a closure problem and no analytical solution is possible. The equations are numerically solved using turbulent models such as K- ε model, k-omega, k-omega SST, Direct Numerical Simulation (DNS) and Large Eddy Simulation (LES). LES and DNS are computationally expensive techniques and require large computational power and simulation time to model the flow, however, K- ε model, k-omega and k-omega SST models are relatively cheaper and widely used with acceptable accuracy [10].

In the model settings, the k-omega SST two-equation viscous model was selected. The model is a combination of the k-omega and K- ε model and forms a new hybrid model. This has the advantage of the near-wall treatment associated with the k-omega model which captures the effect of the sub-viscous layer in the inner layer, along with the standard K- ε model, which captures the outer layer effects [10]. The residual was set to 10^{-5} and except for the continuity equation, all other residuals were below 10^{-5}. However, in addition to residual criteria, the drag and lift force was also monitored on the car-trailer assembly. It was noticed that the results were converging from 300 to 400 iterations and after that, the drag force was oscillating with a small variation. The simulations were, however, run for 600 iterations for each result to ensure that the results were fully converged. Because of the slight fluctuation in the drag after convergence was achieved, a less than ±2% uncertainty in the drag vale was observed.

2.1. CFD Validation

The CFD methodology was validated quantitatively and qualitatively. In qualitative validation, the results of the drag coefficient of models X and Y were compared with the published literature. The analysis of caravans carried by [3, 8] shows a reasonable agreement to the result obtained from the above described CFD methodology. A degree of variation in the simulated and published data cannot be considered as a systematic or repetition error but it is because of the difference in geometric features and dimensions of the model. For the quantitative validation of CFD methodology, a further 1:35th small scale model of a 3D printed tractor-trailer was used to perform experiments in an AF1300 subsonic wind tunnel. The scaled model has a Reynolds number Re of 1M based on the length of the HGV and a blockage ratio of 1%. The same small-scale model was simulated using the same setting in the CFD and 97% similarity was found in the CFD and experimental results. Both, quantitative and qualitative validation has shown reasonable agreement with published and experimental data and has proven the CFD methodology is accurate to carry further analysis.

3. Parametric Optimisation and Analysis

The most important factors affecting drag and fuel consumption are the speed at which the car-trailer assembly is driven and the frontal or projected area of the model. Trailers are usually taller and wider than the car hence, the frontal area is a combination of blockage offered by the height and width of the trailer. Due to internal space-constrained, the height and width cannot be reduced below a certain value. Hence, the projected area can only be controlled by lowering the chassis structure which requires redesigning of the chassis structure and axle. The gap between the rear of the car to the front of the trailer is another important parameter to consider. This allows the flow that is separated from the rear of the car to reattach on the front of the trailer. For the trailer stability and safe vehicle maneuver action, the minimum required gap is 900mm.

Once the designs of the car-trailer assemblies were validated quantitatively and qualitatively, the next step was to compare the performance of the model X and Y trailers. These trailers have similar geometric dimensions and projected areas. Model X has a flat front face however, model Y has a round front. Further to this, a detailed geometric feature optimisation was carried to reduce the overall drag of the car-trailer assemblies. The geometric features that can be modified were the front face, top, and bottom rear sides, the roof of the trailer and gap of the trailer as shown in Figure 5 and Table 2. It is important to note that the design of the car (towing vehicle) was kept constant throughout the analysis.

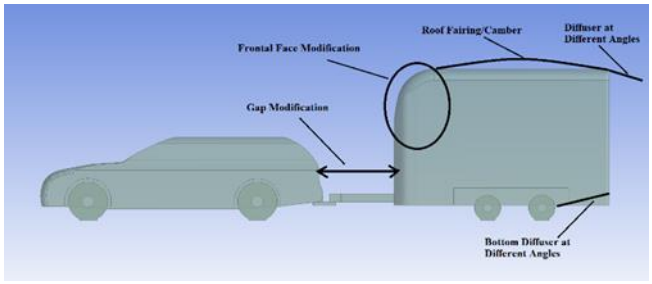

Figure 5 Areas which were modified in this study

Table 2 Parametric changes made in the trailer design

Geometry Type	Minimum	Maximum
Gap/ Drawbar length	b/a= 0.1 Here, b=gap, a= frontal Area of Trailer	b/a=0.4
Front face of the trailer	Height of 500mm	Height of 1500mm
Rear top face of the trailer	-5° angle of diffuser with horizontal	20° angle of diffuser with horizontal
Rear bottom face of the trailer	0° angle with horizontal	8° angle with horizontal
Roof fairing/camber effect	h/l=0.02	h/l=0.08

3.1. Gap/Drawbar Length

In the first modification step, the gap between the rear of the car and the front of the trailer was changed for four different values of b/a (here b=gap/distance between the rear of the car to the front of the trailer, and a=frontal area of the trailer). There is a legal limit on the gap; the minimum length of the gap is set to 0.9m as any closer to this is potentially dangerous for high turns. The gap cannot be more than 1.9m as an increase in length causes high drag and instability issues. Similar gap changes to model X were adopted in model Y as well. The four different values of b/a i.e. 0.1, 0.2, 0.3, and 0.4 were simulated as shown in Figure 6 to find the effect on drag force. The gap in the actual model was 1220mm which was close to the 0.3 b/a ratios.

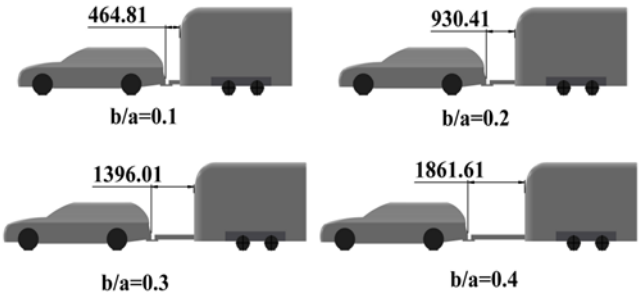

Figure 6 Gap optimisation on model X

The graph of the drag force vs b/a ratio is shown in Figure 7. The drag of the car is changing due to the interference effect of the following trailer body. As the gap between car and trailer is increased, the interference effect starts diminishing hence, the drag of the car starts rising. The total drag of the car-trailer assembly is not equal to the sum of the drag forces of individual bodies. The drag of both, the car and trailer is reduced as compared to their individual drags because of the slip-streaming and Lee-side effect discussed in section 2. The trailer front being in the low-pressure wake region of the car, the drag of the trailer reduces with increased gap and early re-attachment of the flow is observed. The overall drag of the assembly is, however, depends on the shape of the trailer. In model X 0.1 b/a ratio is the optimum value. Contrarily, the optimum position of model Y is determined as 0.2 b/a ratios.

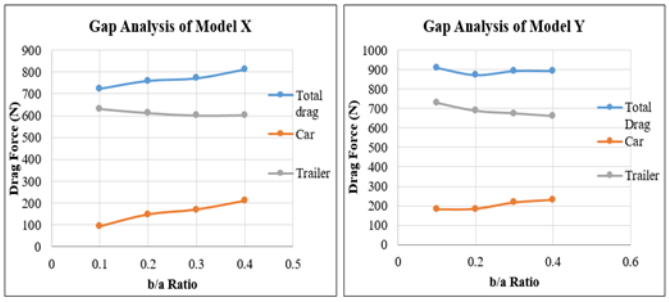

Figure 7 Gap analysis of the car-trailer assemblies at different gap by area ratios

3.2. Frontal Edge and Roof Modification

Shape optimisation was carried to study the flow separation and re-attachment behaviour. For this purpose, the front edge spline of the Model X was modified to three different values. It is important to know that the radius at the front edge was not a single radial curve but it was a continuous curve created using the spline tool. The start point of this curve was moved to three different values i.e. 500mm, 1000mm and 1500mm (Figure 9 & 10). The curve was continually formed in such a manner that it does not have a prominent effect on the frontal area of the trailer. In the second optimisation, the roof camber was tested on the model Y by providing a convex-shaped arch on the roof of the trailer. The length and height of the curve were controlling parameters. A three-point arc was used to generate a curvature on the roof and a ratio of the height of the curve to the distance between endpoints of the curve (h/l) was used as a parameter against the drag force to study the behaviour. The length of the curve was kept constant and height of the arc was controlled in such a way to obtain ratios of 0.02, 0.04, 0.06 and 0.08 with height of 90mm, 180mm, 270mm, and 360mm respectively. As the radius of the curvature was increased, the profile of pressure distribution over the trailer and in the wake region was changed and the peak negative pressure was improved. A high kinetic energy fluid is forced into the wake region which resulted in a reduced wake region as can be seen in Figure 8. Camber also smoothened the leading edge of the trailer and helps flow re-attachment which reduces the drag on the frontal face of the trailer. Additionally, the roof fairing makes the roof shape more streamlined, which results in a delay in separation over the roof of the trailer.

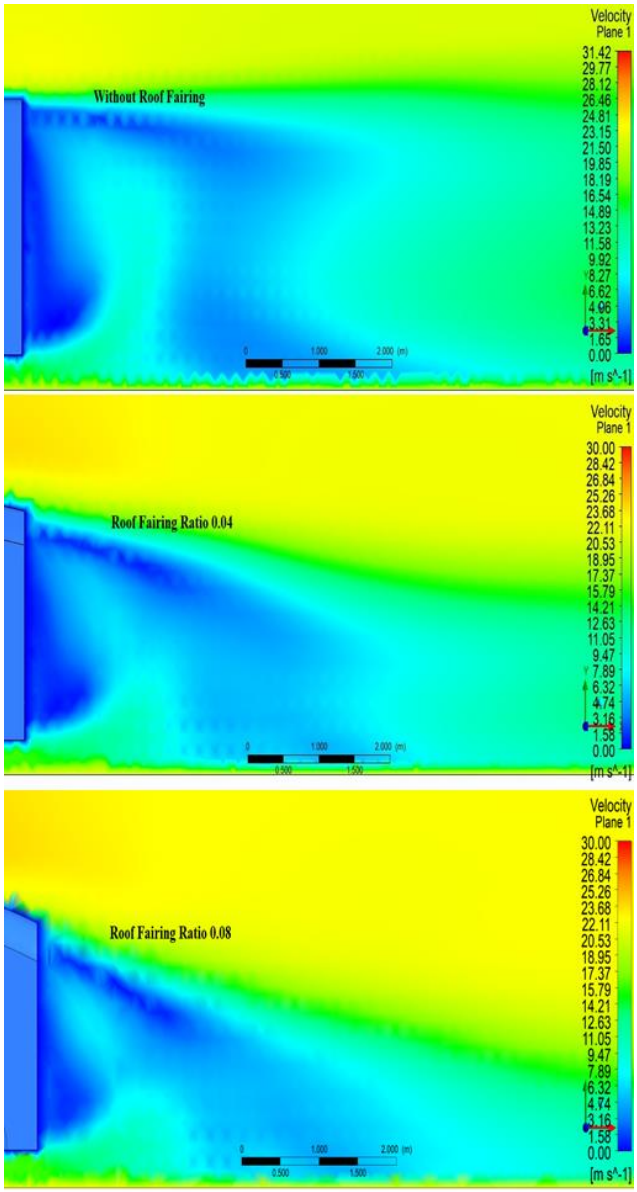

Figure 8 Effect of roof fairing on the wake region in model Y

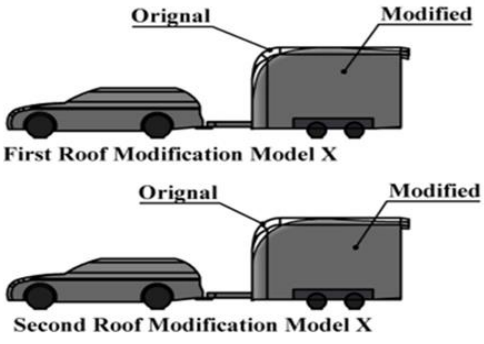

Figure 9 Comparison of original model X with each modified design

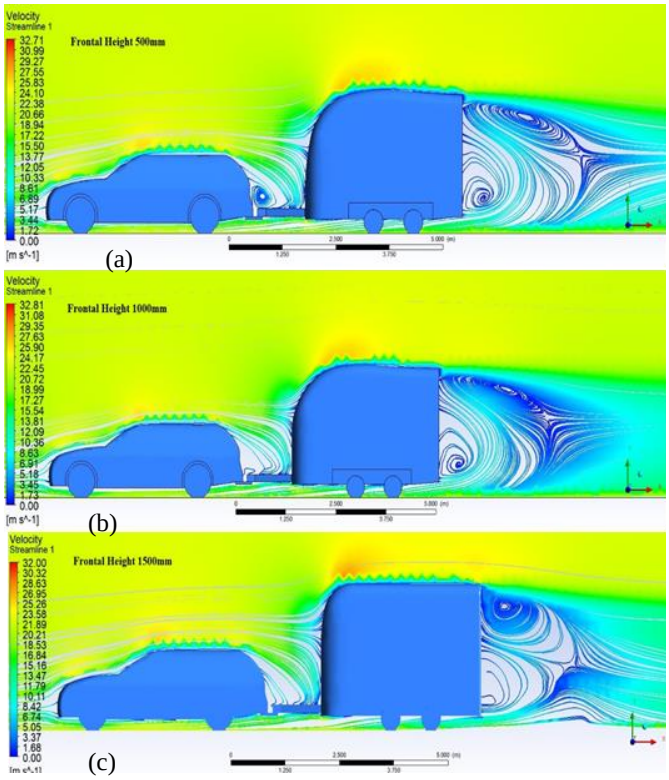

Figure 10 Velocity profile of three different height models (a) 500mm, (b) 1000mm and (c) 1500mm

3.3. Diffuser on the Top Rear End

The drag reduction devices can be expected to show a significant amount of changes in the flow field behaviour. A diffuser of 200mm length was added at the rear end of the roof. Initially the diffuser was added at 0-degree angle. Later the angle was changed to -5, 5, 10, 15, and 20 degrees as shown in Figure 11, in order to find the trend of the drag force and the optimum position of the diffuser. Similar diffuser geometry was tested on both model X and Y trailers. The diffuser has affected the flow structure in the wake region by forcing the high-velocity fluid into the wake region. The wake area has been reduced with the use of an extended diffuser which improves the pressure recovery over the roof and the high-velocity flow forced the shear layer more downwards. When the angle of the diffuser was changed from 0 to -5 degrees upwards, the drag was increased. However, when the angle of the diffuser was changed from 0 to 5, and 10 degrees downward, a significant amount of decrease was observed in the drag value. Further increase in the angle causes flow separation and a slight increase in the drag force. The effect of different diffuser angles on the drag can be seen in the graphs of both models X and Y in Figure 13. The increase in the diffuser angle has a great influence on the pressure distribution on the whole trailer body. Although the pressure is rising after a 10-degree diffuser angle, the distribution of pressure is not favourable to reduce the drag. There is not a significant increase in the drag after a 10-degree diffuser angle in model Y as compared to model X which is mainly due to the curved front face of model Y. The previous study by Cheli, Corradi [23] on tractor-trailer has experienced a similar drag reduction trend of up to 20-degrees.

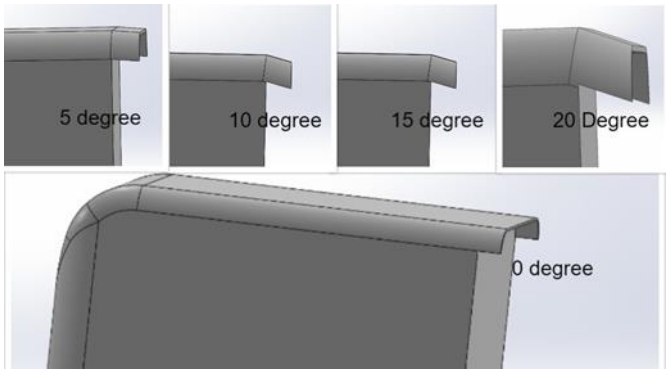

Figure 11 Diffuser at different angles on model X

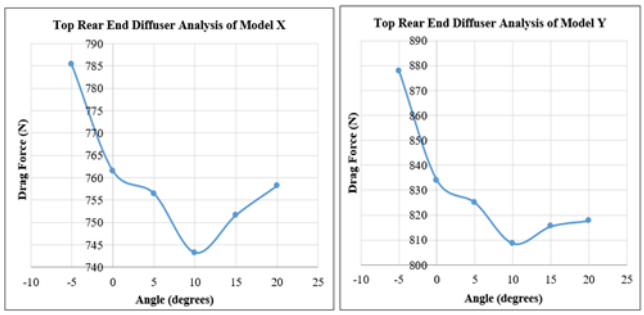

Figure 12 Effect of diffuser angle on drag in both model X and Y

3.4. Diffuser at the Bottom Rear End

Any modification or improvement which would reduce the internal space is less likely to be adopted by the trailer manufacturer. Considering this fact a simple design of the diffuser at the bottom rear end of the trailer was created using extrude cut. The length of the cut was up to the rear axle which was 689mm from the rear face of the trailer. The angle range was selected such that the internal space is unaffected and angles of 0, 2, 4, 6, 8 degrees were simulated for the study of the drag effect. The diffuser was not extended beyond the rear end of the trailer because it was not practical. Most of the trailer manufacturers use rear ramp horse loading, so the extended diffuser can obstruct the opening of the ramp unless the diffuser can be removed or folded. The diffuser was added on both models (X and Y) in the way as explained above. The different configurations of the diffuser can be seen in Figure 12. The drag force was continuously decreasing as the angle of the diffuser was increased from zero to 8 degrees.

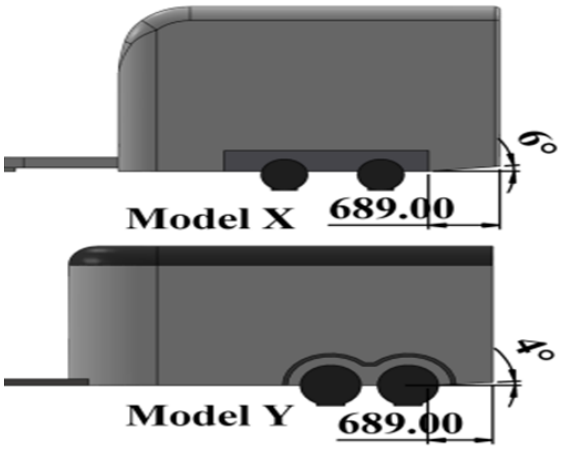

Figure 13 The bottom diffuser at different angles in model X and Y

This decrease in the drag was achieved by the boat tailing effect that allow pressure recovery and improvement in the bottom face pressure profile at the rear edge of the trailer. The pressure contour can be seen in Figure 14. Further increase in the angle may have a positive effect on the drag coefficient but at the same time, it will reduce the internal space and will affect the loading height of the trailer.

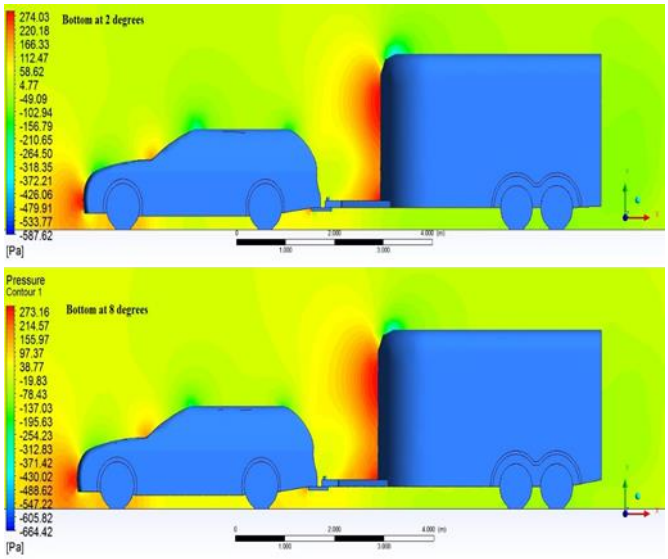

Figure 14 Pressure comparison of zero and 8 degree bottom diffuser angle

4. Discussion and Results

A car carrying a trailer has a significantly greater aerodynamic load than a car driving alone. The separate name selection is used to calculate the drag contributed by each face of the car and trailer. The trailer contributes the most drag, at around 82 percent, compared to the car's contribution of 18 percent. Table 3 represent detail of drag force contributed by each face of the car and trailer and their percentage contribution in the total drag. The drag of the car is significantly reduced by towing a trailer. Rear face of the car generally a large drag contributor, however while towing a trailer, the drag of the rear surface is negative. The negative drag of the car-rear face is because of the pressure rise at the front face of the trailer. In general, the wake pressure of a car travelling alone is negative, but while towing a trailer, the first wake between the car and trailer can be observed as positive in Figure 15. The major drag contributor surfaces in the trailer are trailer-front and rear. The drag of the car-rear surface is dependent on the gap between the car and trailer. As the gap is increased, the interference effect diminishes and the drag of the rear-car surface changes to a positive value. However, the drag contribution of the trailer is reduced up to 74 per cent as the b/a ratio was increased to 0.4. It is observed that the frontal and rear faces of the car and trailer are the major contributors to the drag force. Six per cent of the total drag was contributed by the rotating wheels of the car and trailer. The effect of roof and side faces is minimal as compared to frontal faces. It can be concluded here that the smaller gap provides better fuel efficiency providing the legal requirements are followed.

Table 3: Drag contribution of individual surfaces

Geometry Type	Drag Force (N)	Percentage Contribution
Trailer	645.88	82.70 %
Car	135.1	17.30 %
Car front	145.76	18.66 %
Car rear	-54.24	-6.94 %
Car roof	2.31	0.30 %
Car bottom	5.23	0.67 %
Car left side	2.76	0.35 %
Car right side	2.72	0.35 %
Car wheel	30.57	3.91 %
Trailer front	281.55	36.05 %
Trailer rear	327.94	41.99 %
Trailer roof	4.6	0.59 %
Trailer bottom	2.08	0.27 %
Trailer left side	5.47	0.70 %
Trailer right side	5.34	0.68 %
Trailer wheel	18.83	2.41 %

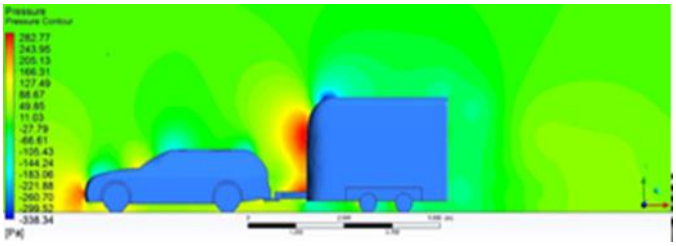

Figure 15 Pressure contour showing positive pressure at rear of the car

The performance of model X is better than model Y as it offers less drag force and provides more space at the front of the trailer. The radius at the leading edge of the model X trailer support reattachment of the flow separated from the rear surface of the car.

However, the front face of model Y directs the flow towards the side faces of the trailer. The vertical height of the frontal face causes a significant increase in the drag force. The curve on the leading edge of the trailer has been positioned at three different locations i.e. 500mm, 1000mm and 1500mm from the bottom face. The results in Figure 16 demonstrate drag reduction from a height of 500mm to 1000mm and from 1000mm to 1500mm, it increased more than double to the prior improvement. Figure 10 represent 500mm case where the drag was higher as compared to 1000mm. This increase in the drag was caused by high flow recirculation in the gap region and a slight increase in the space between the car and trailer while creating a continuous spline. The recirculation provides a low wake pressure on the rear face of the car, which increases drag on the rear face of the car, resulting in an increase in overall drag.

Add-on devices are expected to provide pressure recovery. The diffuser plates added at the rear top and bottom face of the trailer has provided pressure recovery in the wake region. The wake area was reduced with the use of an extended diffuser which improves the pressure recovery over the roof and the high-velocity flow forced the shear layer more downwards. The drag was increased when the diffuser angle was adjusted from 0 to 5 degrees upwards because the wake region was significantly expanded in this situation. However, when the angle of the diffuser was changed from 0, 5, and 10 degrees, a significant amount of decrease was observed in the drag value. Moreover, the change in angle from 15 to 20 degrees caused a slight increase in the drag force for the same reason that has been tested on Ahmed's body. After a specific angle, early flow separation occurs, and it was observed that this angle is dependent on the

vehicle type and geometric dimensions. The diffuser at the rear bottom of the trailer has a positive impact on fuel efficiency. The boat tailing effect provides for pressure recovery and an improvement in the bottom face pressure profile at the trailer's back edge, resulting in a reduction in drag. Further increase in the angle may have a positive effect on the drag coefficient but at the same time, it will reduce the internal space and will affect the loading height of the trailer. Extending the length of the diffuser can help recover more wake pressure and lower the wake area, but it has to be foldable so that it does not interfere with ramp loading.

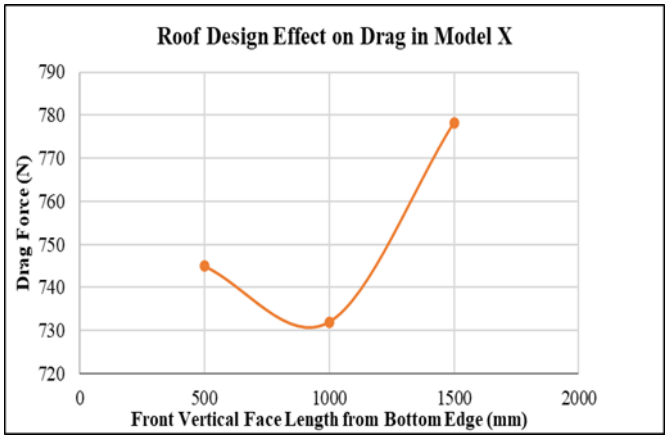

Figure 16 Effect of frontal face vertical height on the overall drag of car-trailer assembly X

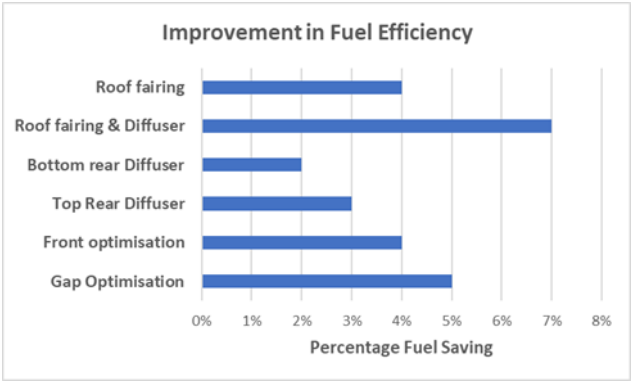

Figure 17 Improvement in fuel saving with different optimisation techniques

At higher speeds, the amount of power required to overcome drag is fairly large. The SAE standard equations published by Charles [24] were used to calculate the fuel consumption. The weight of the car was assumed to be 2500 lb, the tire frictional coefficient to be 0.0061, and the engine efficiency to be 0.24 in the city and 0.3 on the highway. Figure 17 below shows the fuel savings achieved by various shape optimizations and the inclusion of add-on devices. Simple design modifications in the trailer design can save more than 7% in fuel consumption while lowering the CO2 emission into the surrounding environment.

5. Conclusions

CFD based numerical approaches are a powerful tool to study optimisation analysis of the car-trailer combination. Discretising the flow domain into small mesh elements with acceptable quality and low skewness is critical for achieving CFD results closer to the experimental results. In comparison to the Model Y, the Model X offers more living space and better fuel efficiency. The drag reduction can be achieved by minimising the gap between car and trailer and installing the add-on devices. The drag can be reduced by streamlining the front shape of the trailer while maintaining the trailer's internal space. More than 7% fuel saving and reduction in CO_2 emission have been achieved by adopting these design modifications.

6. References

1. De Leon, A., *Improving caravan design by modelling of crosswind*. 2016.
2. Van Leeuwen, P.M., *Computational analysis of base drag reduction using active flow control.* Delft University of Technology, 2009: p. 25-26.
3. Barnard, R.H., *Road vehicle aerodynamic design an introduction 2nd Ed.* 2001, London: Addison Wesley Longman Limited.
4. Malviya, V., et al., *Development of a novel characterisation methodology for the aerodynamic coefficients of a tractor–trailer uit bsed on relative fow agles and vhicle dmensions.* Arabian Journal for Science and Engineering, 2018: p. 4957-4957.
5. Hucho, W.H., *Aerodynamics of road vehicles*. 1998, United States of America: Society of Automotive Engineers.
6. Malviya, V., R. Mishra, and J. Fieldhouse, *CFD Investigation of a noval fuel-saving device for articulated tractor-trailer combination.* Engineering application of Computational Fluid Mechanics Vol 3. No. 4, 2009: p. 587-607.
7. Malviya, V., et al., *Development of a Novel Characterisation Methodology for the Aerodynamic Coefficients of a Tractor–Trailer Unit Based on Relative Flow Angles and Vehicle Dimensions.* Arabian journal for science and engineering (2011), 2018. **43**(9): p. 4957-4975 DOI: 10.1007/s13369-018-3185-3.
8. Schuetz, T., *Aerodynamics of road vehicles*. Fifth ed. 2016, Warrendale, Pennsylvania, USA: SAE International.
9. Hoerner, S., *Fluid-dynamic drag, 2nd edition*. 1965: Midland park, N.J.
10. Aftab, S.M., et al., *Turbulence Model Selection for Low Reynolds Number Flows.* PLoS One, 2016. **11**(4): p. e0153755 DOI: 10.1371/journal.pone.0153755.
11. Asim, T. and R. Mishra, *Computational fluid dynamics based optimal design of hydraulic capsule pipelines transporting cylindrical capsules.* Powder technology, 2016. **295**: p. 180-201.
12. Argyropoulosa, C.D. and N.C. Markatos, *Recent advances on the numerical modelling of turbulent flows.* Applied mathematical modelling, 2015: p. 693-732.
13. Giancarlo, A., *Reynolds-Averaged Navier-Stokes equations for turbulence modeling* . Applied Mechanics Review,, 2009: p. 1-20.
14. Rajendran, S. and K. Purushothaman, *Design and analysis of drag force and fuel consumption in small vehicles using CFD.* International Journal of Applied Engineering Research, 2015: p. 10(ISSN 0973-4562):5792 - 5796.
15. Vandromme, D.R., *Overview of turbulence model for CFD in industry.* Industrial computational fluid dynamics, lectture series 1995-03,, 1995.
16. EL Tahry, S.H. and D.H. Haworth, *A critical review of turbulence models for application in the automotive industry.* AIAA Paper 91-0516, 29th aerospace sciences meeting, Reno, Nev., 1991: p. 7-10.
17. Menter, F.R., *Zonal two equation k-ω turbulence models for aerodynamic flows.* AIAA Paper 93-2906., 1993.
18. Buchheim, R., K.R. Deutenbach, and H.J. Luckoff, *Necessaity and premises fro reducing the aeropdynamic drag of future passsenger cars.* SAE Transactions, vol. 90, 1981: p. 758-771.

19. Barnard, R.H. and D.R. Philpott, *Aircraft Flight*. 1989, Harlow: Longman.
20. Gunes, D., *Drag coefficient prediction analysis for heavy duty trucks, Progress in Computational Fluid Dynamics,*. Progress in Computational Fluid Dynamics An International Journal, 2007: p. vol. 7, no. 8, .
21. Pointer, W.D., *Evaluation of CFD code capabilities for prediction of heavy vehicle drag coefficients,*. Fluid Dynamics Conference and Exhibit, 2004: p. AIAA-2004-2254, .
22. Muhammad Atif, A.M.A., Rakesh Mishra, *Management of fuel consumption and emissions of heavy goods trucks.* ICMIAM conference 2021, 2021.
23. Cheli, F.R., E. Corradi, and T. Sabbioni, G., *Wind tunnel tests on heavy road: cross wind induced loads—Part 1*. Journal of Wind Engineering and Industrial Aerodynamics, 2011: p. 1000-1010.
24. Mendler, C., *Equations for Estimating and Optimizing the Fuel Economy of Future Automobiles.* SAE transactions, 1993. **102**: p. 2367-2373.